ACS Photonics

Article

pubs.acs.org/journal/apchd5

Amplitude- and Phase-Controlled Surface Plasmon Polariton Excitation with Metasurfaces

Holger Mühlenbernd,[†] Philip Georgi,[†] Nitipat Pholchai,[‡,§] Lingling Huang,[∥] Guixin Li,[⊥] Shuang Zhang,[⊥] and Thomas Zentgraf*[,†]

[†]Department of Physics, University of Paderborn, Warburger Straße 100, Paderborn D-33098, Germany

[‡]Department of Industrial Physics and Medical Instrumentation and [§]Lasers and Optics Research Group, King Mongkut's University of Technology North Bangkok, 1518 Pibulsongkram Road, Bangkok 108100, Thailand

[∥]Beijing Institute of Technology, No. 5 South Zhongguancun Street, Beijing 100084, China

[⊥]School of Physics & Astronomy, University of Birmingham, Birmingham B15 2TT, United Kingdom

Supporting Information

ABSTRACT: Surface plasmon polaritons (SPPs) have shown high potential for various applications in various fields, ranging from physics, chemistry, and biology to integrated photonic circuits due to their the strong confinement of light to the metal surface. Exciting an SPP from a free-space photon in a controllable manner is an essential step toward more complex and integrated applications. Methods for coupling photons to SPPs are numerous, but in order to control the amplitude and phase of an SPP, most of these methods require bulky or multiple optical components or sensitive adjustments that are difficult to control. Here we present a novel approach for an independent control of the amplitude and phase of an SPP excited by a normally incident beam using a metasurface. The full control in amplitude and phase is achieved via the polarization state and polarization orientation angle of the electrical field of the incoming light. We experimentally demonstrate the functionality of such a metasurface consisting of periodic nanoantennas for the excitation of SPPs at a metal−dielectric interface. Our approach opens up new ways for coherently controllable integrated plasmonic circuits that can be used in conjunction with fast dynamic polarization modulation techniques.

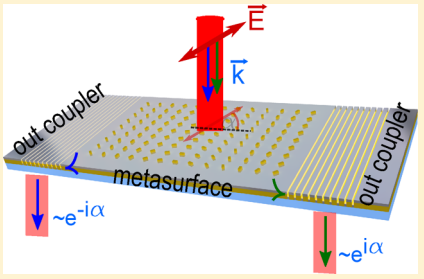

KEYWORDS: *plasmonics, SPP excitation, optical mode excitation, metasurface, amplitude and phase control*

Surface plasmon polaritons (SPPs) are electromagnetic excitations propagating at the interface between a dielectric and a conductor, evanescently confined in the perpendicular direction of their propagation.[1] The number of applications that utilize SPPs has increased tremendously during the last decades, including energy harvesting,[2] coupler or modulator in integrated optics,[3−7] biosensing,[8,9] subdiffraction imaging,[10] and quantum optics.[11] The great interest in SPPs results from their unique abilities such as the strong confinement of the field to the interface and their unique dispersion relation. However, the mismatch of the SPP momentum to that of free-space photons prevents light from free space from coupling efficiently into an SPP mode, making it necessary to add periodic structures or to modify the dispersion relation at the interfaces to satisfy momentum conservation. To date, several different approaches have been developed to excite SPPs for various applications. More classical techniques such as the Kretschmann[12] or the Otto[13] configuration use bulky prisms to alter the momentum of the incoming light beam through dispersion. These techniques are cumbersome to implement and impractical for flat optics technology and optical circuits with vertical integration. Moreover, momentum matching with prisms is sensitive to the incident angle of the incoming light. Gratings, on the other hand, while able to couple free-space light into an SPP mode by providing an additional wave vector for momentum matching, lack the ability to dynamically control the phase or amplitude of the excited SPPs.[14,15] Recently it has been demonstrated that resonant plasmonic structures such as magnetic dipole antennas can also be used for directionally coupling light into SPPs.[16,17] Such directional coupling was also demonstrated by utilizing an abrupt phase change due to a Pancharatnam−Berry phase for nanoapertures in the metal film instead of the dipole antennas.[18] However, the efficiency is relatively low. Nonetheless, it demonstrates that the polarization state of the excitation light beam is a convenient parameter for controlling the direction of the SPP excitation. Moreover, these metasurfaces are thin, scalable, and capable of being easily integrated. Previous studies so far have not demonstrated the full control of both excitation amplitude and phase of SPPs independently and simultaneously, which is a crucial feature for launching light into integrated optical circuits. Here we present a novel approach for SPP excitation based on a scalable ultrathin plasmonic metasurface that is able to provide a fully variable and independent control of the excitation strength and phase for SPPs without modification of

Received: September 20, 2015
Published: December 23, 2015

DOI: 10.1021/acsphotonics.5b00536
ACS Photonics 2016, 3, 124−129

the surface topology. Our approach utilizes arrays of subwavelength plasmonic dipole nanoantennas with a local abrupt phase discontinuity[19] on top of a metal−insulator substrate, which is illuminated by an optical beam at normal incidence. Since the amount of the phase change introduced by the local antennas depends on the polarization state and the orientation of the dipole antennas, such metasurfaces can alter the phase of the excited SPPs either by the geometry (rotation) of the nanoantennas themselves or by the orientation of the linear polarization state of the incident light. Furthermore, by changing the polarization state of the light from linear to elliptical and circular we show that we have the extra freedom to control the amplitude of the SPP excitation.

CONCEPT

For our demonstration of amplitude- and phase-controlled SPP excitation we utilize an array of subwavelength plasmonic dipole nanoantennas in close proximity to a gold surface.[14,20,21] Such structures can efficiently couple free-space light to SPPs. In contrast to most previously used designs, which utilized a gradient in the lattice constant, we arranged the nanoantennas in a periodic pattern with a constant gradient of orientation angle φ along the x-direction as shown in Figure 1a. To

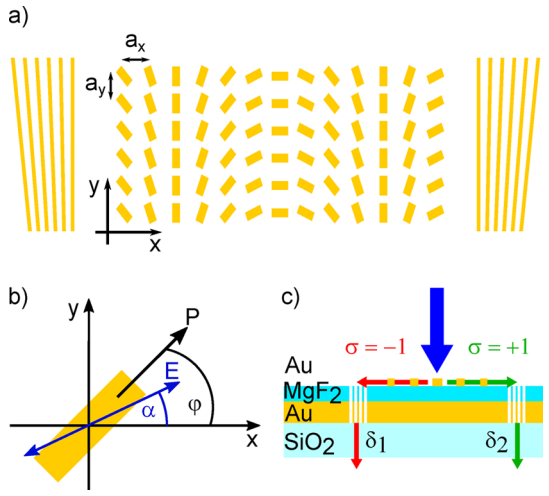

Figure 1. Design schematics of the metasurface. (a) Top view of the metasurface with out-coupler gratings on two sides and a nanoantenna array in the middle. The periodicity of the gratings has been altered along the y-direction to tune the operation wavelength for the out-coupled light. (b) Geometry of a single antenna. The orientation angle φ describes the direction of the antenna polarization P compared to the x-axis. The blue arrow corresponds to the oscillation direction of the electrical field E for a linearly polarized incident beam with the angle α to the x-axis. (c) Cross section of the structure with the etched gratings and the light paths (arrows). Blue arrow represents the polarized incident light. Red arrows represent the light paths for LCP light ($\sigma = -1$), and green arrows the RCP light ($\sigma = +1$). The phase of the out-coupled light is labeled with δ_i, where $i = 1, 2$ corresponds to the two out-coupling channels.

efficiently couple the incoming free-space light into an SPP wave, it is important to keep the distance between the nanoantennas and the gold surface as small as possible because of the evanescently confined nature of an SPP. Within the antenna array each nanoantenna scatters constructively coupled light into the SPP mode if the momentum conservation condition is fulfilled. The scattered electrical field of each single dipole can be decomposed into two circularly oscillating components. One component has the same helicity as the incident light, and the other one with opposite helicity carries an additional phase of 2φ, where φ is the orientation angle of the nanoantenna in the local coordinate system (Figure 1b).[19] Because of its geometrical nature (Pancharatnam−Berry phase), this additional phase is independent of the resonance frequency of the nanoantennas, and therefore the phase-controlled excitation is possible over a broad wavelength spectrum.

Since the periodic antenna array acts like a grating coupler to couple light into an SPP mode, it is necessary to fulfill the momentum conservation:

$$k_{SPP} = k_\Gamma + \sigma\Delta k = m\frac{2\pi}{a_x} + \sigma\frac{2\Delta\varphi}{a_x} \quad (1)$$

Here k_{SPP} is the in-plane wave vector of the propagating SPP, k_Γ the wave vector of the periodic structure of antennas, and $\sigma\Delta k$ the momentum generated by the polarization-dependent geometrical phase effect of the antennas. The momentum of the periodic arrangement is given by the diffraction order m and the lattice constant a_x in the x-direction, whereas the momentum due to the geometrical phase effect is given by the orientation-dependent geometrical phase gradient $2\Delta\varphi/a_x$ (with the rotation angle $\Delta\varphi$ between two neighboring antennas). The factor σ represents the helicity of circularly polarized light ($\sigma = \pm 1$ for right circularly polarized (RCP) and left circularly polarized (LCP) light, respectively).

To fulfill the momentum conservation, a periodic nanoantenna array without the additional phase gradient ($\Delta\varphi = 0$) would be sufficient. For this case the array would act like a regular grating coupler and unidirectional SPP excitation or phase control between both counter-propagating SPP waves for a normally incident light beam could not be obtained. However, the additional helicity and geometrical phase-dependent momentum $\sigma\Delta k$ give us the opportunity to couple light unidirectionally from the free space to the SPP mode since it will break the symmetry of the periodic pattern for circularly polarized light (Figure 1c). The polarization-dependent unidirectionality is illustrated by the dispersion curve of SPPs and the momentum matching condition for the periodic antenna array with its wave vector k_Γ and the polarization-dependent momentum Δk (Figure 2). Because of the

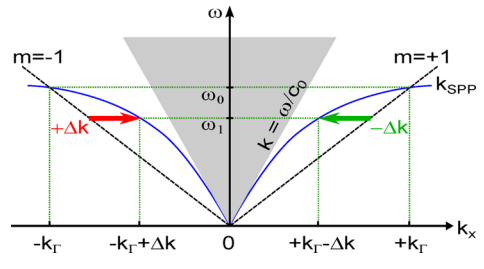

Figure 2. Dispersion curve of SPPs at the MgF_2/gold interface (blue solid line) and the light cone of free-space light (gray area). The black dotted line represents the wave vector k_Γ of the periodic antenna field, which acts as a grating. Only with the polarization-dependent momentum Δk due to the geometrical phase of the antennas can the phase matching condition for RCP (green arrow) or for LCP (red arrow) be fulfilled for the given frequency ω_1.

DOI: 10.1021/acsphotonics.5b00536
ACS Photonics 2016, 3, 124−129

additional momentum $\pm \Delta k$, the momentum conservation for circularly polarized light at the frequency ω_1 can be fulfilled only for one propagation direction (one branch of the dispersion curve) of the SPPs: For $\Delta\varphi$ being a negative value and RCP (LCP) incident light the momentum conservation would lead to a propagating SPP wave along the dielectric–metal interface only to the right (left) direction (as illustrated in Figure 1c). Hence, by using a superposition of the two circular polarization states of the incoming light, it is possible to control the excitation ratio between the two SPP waves propagating in opposite directions. This effect was already demonstrated for an array of small nanoapertures in the metal film, demonstrating unidirectional SPP excitation by circularly polarized light.[18] However, a nanoantenna array in close proximity to the metal interface has the advantage of easier fabrication and higher coupling efficiency.[17]

For controlling the excitation phase of the SPPs launched at these nanoantenna arrays we can utilize linearly polarized incident light. Since the polarization (oscillation direction of the electrical field) is in general easy to change by wave plates, this will provide us an easy-to-control parameter for tailoring the phase of the propagating SPP wave. To understand such a behavior, we decompose the scattered incident field at the nanoantennas into RCP and LCP light, which will contain a constant phase relation of 2α between the two polarizations. Here, α is the angle of the incident linear polarization orientation with respect to the x-axis (see Figure 1b). Using E_R and E_L for the amplitudes of the RCP and LCP electrical field in a circular polarization vector basis, the incident electric field at the antennas is therefore given by

$$\vec{E} = E_R \vec{e}_R + E_L e^{i2\alpha} \vec{e}_L \quad (2)$$

For this incident field we can derive the induced material polarization P in each nanoantenna that will be responsible for coupling the scattered light into the SPPs (see Supporting Information):

$$\vec{P} = \frac{\alpha_e}{2}([E_L e^{i2(\alpha-\varphi)}]\vec{e}_R + [E_R e^{i2\varphi}]\vec{e}_L) \quad (3)$$

whereas α_e is the electrical polarizability of a single nanoantenna. Since P will act as the source term for the SPPs, a linearly polarized incident beam will result in an equal distribution of counter-propagating SPP excitations but with different phases between them, depending on the orientation angle φ of the nanoantenna and the polarization orientation α of the incident field.

RESULTS AND DISCUSSION

In the following, we experimentally prove our concept by demonstrating independently the helicity-dependent unidirectional propagation and the polarization-orientation-dependent induced phase of the SPP excited from a free-space beam. The sample was fabricated on a Suprasil 300 quartz glass substrate with deposition of 1 nm chromium as adhesion layer and 130 nm thick gold as metal surface covered by 30 nm thick MgF_2 as dielectric spacer layer for the metasurfaces on top. As we couple the SPPs back to the far field for measurement by a regular grating coupler, the gold substrate layer needs to be thick enough to prevent direct transmission of incoming light through the metal film (which would give a strong background signal). On the other hand if the film becomes too thick, it is more difficult to etch gratings with high aspect ratio into the metal. Therefore, we choose 130 nm as an acceptable metal layer thickness.

To probe the propagating SPPs, we utilized a grating on each side of the nanoantenna array to couple the surface waves back into the far field for detection of the intensity and phase at a CCD camera. The distance between the edge of the antenna array and the grating is 18 μm. The antennas have a size of about 200 × 100 nm^2 with a thickness of about 33 nm and are periodically arranged with a lattice constant of a_x = 650 nm and a_y = 500 nm, respectively (Figure 3). Each row along the

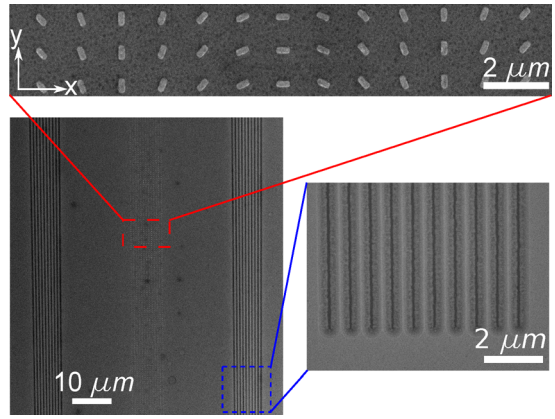

Figure 3. Scanning electron microscopy images of the sample with the gold nanoantenna array and the etched gratings on both sides. The image at the top shows a magnified view of three complete rows of the nanoantennas. The image to the right shows parts of the right gratings, which couple the SPP to the far field.

x-direction of the antenna array consists of 13 antennas with a geometrical rotation of $\Delta\varphi = \pi/8$ between two nearest antennas. The antennas are aligned symmetrically to the center of the array to avoid an additional phase shift between for the counter-propagating SPPs.

To demonstrate the ability to control the amplitude of SPP excitation, we used the optical setup schematically illustrated in Figure 4. The laser beam at 800 nm is focused on the metasurface to form a spot size of about 5 μm. The excited SPPs couple through the grating coupler back into the far field.

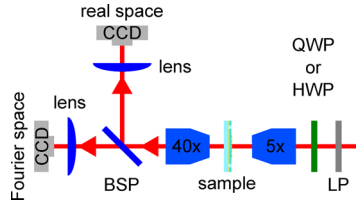

Figure 4. Schematics of the experimental setup for measuring the helicity-dependent SPP excitation and the polarization-orientation-dependent phase. For the excitation of the SPPs a laser beam is filtered through a linear polarizer (LP) to avoid unpolarized light. Then, a quarter-wave plate (QWP) for the generation and control of elliptically polarized light or a half-wave plate (HWP) for the control of the oscillation direction of linearly polarized light is used, respectively. Two microscope objectives focus the laser beam onto the antenna array and collect the light out-coupled by the gratings into the far field. A beam splitter (BSP) splits the imaging paths to the two cameras, where one images the real space and one the Fourier space of the sample surface.

DOI: 10.1021/acsphotonics.5b00536
ACS Photonics 2016, 3, 124–129

The far-field radiation is collected via an objective lens (40×/0.60) and imaged to a CCD camera.

The out-coupled light forms bright spots in the camera image at the positions of out-couple gratings, where the intensity of these spots is proportional to the intensity of the counter-propagating SPPs. By rotating the quarter-wave plate in front of the focusing lens the polarization state of the incoming light can be tuned continuously from vertical linear polarization through elliptical and circular polarizations, back to the vertical linear polarization. For each polarization state the light intensities at the two out-coupling gratings are recorded at the CCD camera and finally integrated over the grating area (Figure 5). The

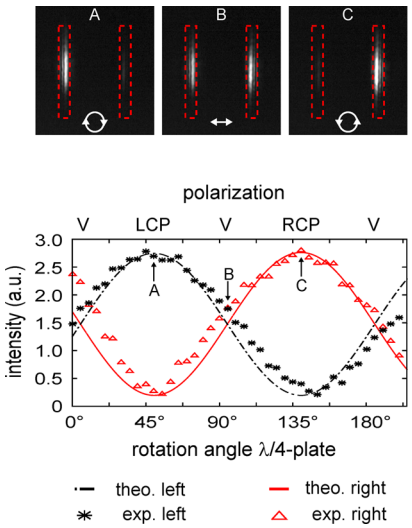

Figure 5. Experimental demonstration of continuous tuning of relative amplitudes of the SPPs measured from the left and the right gratings. (a) Recorded real-space images of the sample surface for three different polarization states of the incident light. The red dotted lines indicate the positions of the gratings. (b) Integrated intensity from the right (red triangles) and left (black stars) gratings over the rotation angle of the quarter-wave plate. The upper x-axis shows the corresponding polarization states of the incident light. The lines show the theoretical predictions for the intensities (black dashed line for the left grating, red solid line for the right grating).

experimental results show clearly that the intensity at the two gratings varies with the ellipticity of the incoming light. For the two circular polarization states we observe a unidirectional SPP excitation where the intermediate polarization states allow the continuous tuning of the amplitude of the SPP excitation strength. The results are in good agreement with our theoretical prediction (for details see the Supporting Information).

In the following we will focus on the linear polarization states so that SPPs are excited equally in both directions of the nanoantenna array (for example see measurement B in Figure 5). By changing the orientation of the linearly polarized incident light using a half-wave plate (instead of the quarter-wave plate), the real-space images of the gratings display the same intensity (not shown) for all linear polarization orientations due to equal excitation of SPPs in both $+x$- and $-x$-direction. However, eq 3 showed a phase dependence on the orientation angle α of the linear polarization state. Hence the relative phase between the two SPPs propagating in opposite directions should change with the orientation of the half-wave plate. To gain information about the phase relation of the SPPs, we image the Fourier space of the surface instead of the real space. This provides us with the possibility to detect the interference of the light coming from both gratings and thereby measure the relative phase between the counter-propagating SPPs. The obtained Fourier image on the CCD camera is therefore analogous to the well-known double-slit experiment, which shows a shift of the fringe patterns when the relative phase between both slits is changed.

Without loss of generality, we compare our experiment with the results of a double-slit experiment assuming two light beams with the same intensity. The amplitudes E_R and E_L are equal and are set to the value $\frac{E_0}{\sqrt{2}}$. The total intensity due to the sum of the two sources can then be expressed as a function dependent on the polarization orientation angle α:

$$I(\alpha) \propto \left(\frac{\alpha_e E_0}{2}\right)^2 sin^2(\alpha - 2\Phi) \tag{4}$$

where Φ is a reference offset phase, which depends on the symmetry of the antenna array with respect to the illumination beam (see Supporting Information for details). Figure 6a shows the simulated field distribution of the electrical field along the MgF_2/Au interface for the two orthogonal linear polarizations of the incident field. From these simulations it is obvious that a $\pi/2$ phase shift of the SPPs for each direction occurs when the polarization angle is changed by $\alpha = 90°$, which results in an entire phase shift between the two counter-propagating SPPs of $\Delta = 2\alpha = \pi$.

The intensity function (eq 4) leads to interference fringes in the Fourier space of the sample surface such as the ones shown in Figure 6b. In these images, it is clearly visible that the interference pattern shifts for different polarization angles of the incident light. An analysis of these interference patterns allows us to determine the intensity change (Figure 6c) at a particular position of the CCD camera (marked by the white line in Figure 6b), which corresponds well to eq 4. Hence the obtained phase difference Δ of the counter-propagating SPPs follows our predicted phase introduced by the nanoantennas (eq 3). Figure 6d summarizes the results by showing the obtained phase difference Δ between the two counter-propagating SPPs, which exhibits a linear relationship with the incident polarization angle. Hence the phase shift for an SPP with respect to the excitation field is $\Delta/2$. This method thus demonstrates a simple linear control of the phase of SPPs with the incident linear polarization angle.

CONCLUSION

In this work we have demonstrated both helicity-dependent unidirectional SPP excitation and polarization-controlled phase modulation of SPPs based on a metasurface placed in close proximity to the metal interface. Through an interference experiment we experimentally verified that the phase difference between two counter-propagating SPPs can be tuned continuously with the incident polarization state. Combining both effects such metasurfaces based on nanoantenna structures are able to simultaneously tailor both the intensity and phase of SPPs. In contrast to other concepts with a high excitation efficiency of the SPP modes (here we reach about 4% at the design wavelength of 800 nm for RCP light; see Supporting Information), our work goes beyond previous works that only generated controllable unidirectional SPPs.[17,18] More importantly, the concept we demonstrated here is based on a general concept of a geometrical phase change due to a Pancharatnam–Berry phase,[19−24] which means it is not necessarily limited to an

DOI: 10.1021/acsphotonics.5b00536
ACS Photonics 2016, 3, 124−129

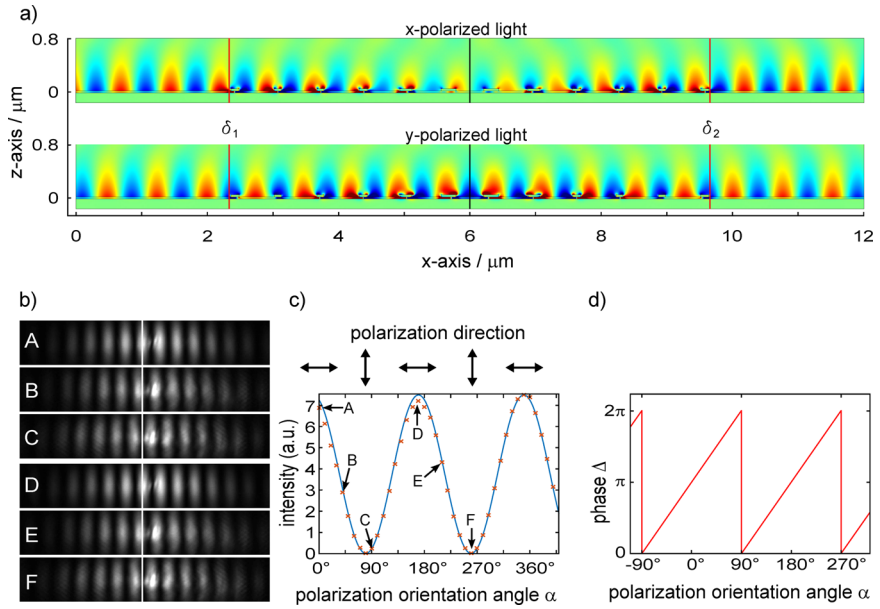

Figure 6. Theoretical calculations and experimental demonstration of continuous tuning of the relative phase between counter-propagating SPPs. (a) Simulated field distribution of the electrical field (E_z) along the metasurface for two orthogonal polarization states of the incoming light with the beam center at 6 μm (black line). (b) Measured Fourier plane images of the sample surface showing a shift of the resulting interference fringes from the two gratings when the orientation angle α of the incident linear polarization is changed. The white line marks the position that is used to evaluate the intensity. (c) Experimentally obtained value (crosses) and the theoretical model (solid line) of the signal intensity at the marked position as a function of the orientation angle α. The double-headed arrows on top represent the corresponding polarization of the incident light. (d) Linear relationship between the phase difference Δ of the counter-propagating SPPs and the polarization angle α of the incident field, which demonstrates a simple linear control of the phase of the SPPs using the incident linear polarization orientation.

SPP excitation, but can also provide identical coupling, e.g., to modes in dielectric optical waveguides.[4] The nanoantenna arrays could also be used as a waveguide coupler to couple free-space light into or out of an optical waveguide and to generate a relative phase or an amplitude difference just by controlling the polarization state of the light. This would allow reaching any point on the Poincaré sphere, which is a requirement for many applications in the fields of quantum optics and state engineering. Therefore, it is unimportant if the quantum system is given by a single photon source or a quantum bit. Our concept has the potential to simplify the state engineering and to give new impulses to quantum optics. Furthermore, the combination of the metasurfaces with thin films of liquid crystals for obtaining controlled polarization changes could lead to a fully integrated optical device, which would open up a new gateway for integrated optics.[25]

METHODS

Fabrication of the Metasurface. A quartz glass substrate (Suprasil 300, Heraeus) has been coated with a 130 nm thick gold film by electron beam evaporation. To etch the out-couple gratings into the gold layer, a hard mask is necessary. An electron beam resist (ARP 671.02; PMMA 950k) of 200 nm is sufficient to protect the metal surface during the dry etching process. The lines that form the out-coupler are patterned into the resist using electron beam lithography (Raith Pioneer system). Each grating consists of 10 lines with a width of 90 nm and a length of 100 μm. The periodicity has been altered along the y-direction ranging from 730 to 841 nm to tune the operation wavelength of the gratings around 800 nm. The lines are etched into the gold layer using an argon sputter etch process by a plasma etching system (Oxford Instruments Plasmalab System 100). The MgF_2 spacer layer is deposited after etching the gratings and removing the photoresist by electron beam evaporation at 100 °C. The antennas are patterned on top of the MgF_2 layer using electron beam lithography (Raith Pioneer system) and a lift-off technique.

ASSOCIATED CONTENT

Supporting Information

The Supporting Information is available free of charge on the ACS Publications website at DOI: 10.1021/acsphotonics.5b00536.

Detailed calculations concerning the theoretical intensity plots of the continuous tuning of the relative phase and the relative amplitude (PDF)

AUTHOR INFORMATION

Corresponding Author

*E-mail: thomas.zentgraf@uni-paderborn.de.

Notes

The authors declare no competing financial interest.

ACKNOWLEDGMENTS

The authors would like to acknowledge the continuous support by Cedrik Meier for providing his electron beam lithography system for sample fabrication. The work was financially supported by the DFG Research Center TRR142 "Tailored nonlinear photonics" and the DFG Research Training Group GRK1464. T.Z. acknowledges support from the European Commission under the Marie Curie Career Integration Program.

DOI: 10.1021/acsphotonics.5b00536
ACS Photonics 2016, 3, 124−129

REFERENCES

(1) Maier, S. A. *Plasmonics—Fundamentals and Applications*; Springer: New York, 2007.

(2) Atwater, H. A.; Polman, A. Plasmonics for improved photovoltaic devices. *Nat. Mater.* **2010**, *9*, 205−213.

(3) Nikolajsen, T.; Leosson, K.; Bozhevolnyi, S. I. Surface plasmon polariton based modulators and switches operating at telecom wavelengths. *Appl. Phys. Lett.* **2004**, *85* (24), 5833−5835.

(4) Arango, F. B.; Kwadrin, A.; Koenderink, A. F. Plasmonic Antennas Hybridized with Dielectric Waveguides. *ACS Nano* **2012**, *6* (11), 10156−10167.

(5) Gao, W.; Shi, G.; Jin, Z.; Shu, J.; Zhang, Q.; Vajtai, R.; Ajayan, P. M.; Kono, J.; Xu, Q. Excitation and Active Control of Propagating Surface Plasmon Polaritons in Graphene. *Nano Lett.* **2013**, *13*, 3698−3702.

(6) Melikyan, A.; Lindenmann, N.; Walheim, S.; Leufke, P. M.; Ulrich, S.; Ye, J.; Vincze, P.; Hahn, H.; Schimmel, Th.; Koos, C.; Freude, W.; Leuthold, J. Surface plasmon polariton absorption modulator. *Opt. Express* **2011**, *19* (9), 8855−8869.

(7) Charbonneau, R.; Lahoud, N. Demonstration of integrated optics elements based on long-ranging surface plasmon polaritons. *Opt. Express* **2005**, *13* (3), 977−984.

(8) Homola, J. Present and future of surface plasmon resonance biosensors. *Anal. Bioanal. Chem.* **2003**, *377*, 528−539.

(9) Anker, J. N.; Hall, W. P.; Lyandres, O.; Shah, N.C.; Zhao, J.; Van Duyne, R. P. Biosensing with plasmonic nanosensors. *Nat. Mater.* **2008**, *7*, 442−453.

(10) Gramotnev, D. K.; Bozhevolnyi, S. I. Plasmonics beyond the diffraction limit. *Nat. Photonics* **2010**, *4*, 83−91.

(11) Tame, M. S.; McEnery, K. R.; Özdemir, S. K.; Lee, J.; Maier, S. A.; Kim, M. S. Quantum plasmonics. *Nat. Phys.* **2013**, *9*, 329−340.

(12) Kretschmann, E. Die Bestimmung der Oberflächenrauhigkeit dünner Schichten durch Messung der Winkelabhängigkeit der Streustrahlung von Oberflächenplasmaschwingungen. *Opt. Commun.* **1974**, *10* (4), 353−356.

(13) Otto, A. Excitation of Nonradiative Surface Plasmon Waves in Silver by the Methode of Frustrated Total Reflection. *Eur. Phys. J. A* **1968**, *216*, 398−410.

(14) Dolev, I.; Arie, A. Surface-Plasmon Holographic Beam Shaping. *Phys. Rev. Lett.* **2012**, *109*, 203903.

(15) Bar-Lev, D.; Arie, A.; Scheuer, J.; Epstein, I. Efficient excitation and control of arbitrary surface plasmon polariton beams using one-dimensional metallic gratings. *J. Opt. Soc. Am. B* **2015**, *32* (5), 923−932.

(16) Liu, Y.; Palomba, S.; Park, Y.; Zentgraf, T.; Yin, X.; Zhang, X. Compact Magnetic Antennas for Directional Excitation of Surface Plasmons. *Nano Lett.* **2012**, *12*, 4853−4858.

(17) Pors, A.; Nielsen, M. G.; Bernardin, T.; Weeber, J. C.; Bozhevolnyi, S. I. Efficient unidirectional polarization-controlled excitation of surface plasmon polaritons. *Light: Sci. Appl.* **2014**, *3*, e197.

(18) Huang, L.; Chen, X.; Bai, B.; Tan, Q.; Jin, G.; Zentgraf, T.; Zhang, S. Helicity dependent directional surface plasmon polariton excitation using a metasurface with interfacial phase discontinuity. *Light: Sci. Appl.* **2013**, *2*, e70.

(19) Huang, L.; Chen, X.; Mühlenbernd, H.; Li, G.; Bai, B.; Tan, Q.; Jin, G.; Zentgraf, T.; Zhang, S. Dispersionless Phase Discontinuities for Controlling Light Propagation. *Nano Lett.* **2012**, *12*, 5750−5755.

(20) Pors, A.; Nielsen, M. G.; Eriksen, R. L.; Bozhevolnyi, S. I. Broadband focusing mirrors based on plasmonic gradient metasurfaces. *Nano Lett.* **2013**, *13*, 829−834.

(21) Sun, S.; Yang, K.-Y.; Wang, C.-M.; Juan, T.-K.; Chen, W. T.; Liao, C. Y.; He, Q.; Xiao, S.; Kung, W.-T.; Guo, G.-Y.; Zhou, L.; Tsai, D. P. High-Efficiency Broadband Anomalous Reflection by Gradient Meta-Surfaces. *Nano Lett.* **2012**, *12*, 6223−6229.

(22) Yu, N.; Genevet, P.; Kats, M. A.; Aieta, F.; Tetienne, J. P.; Capasso, F.; Gaburro, Z. Light Propagation with Phase Discontinuities: Generalized Laws of Reflection and Refraction. *Science* **2011**, *334*, 333−337.

(23) Bornzon, Z.; Biener, G.; Kleiner, V.; Hasman, E. Space-variant Pancharatnam-Berry phase optical elements with computer-generated subwavelength gratings. *Opt. Lett.* **2002**, *27* (13), 1141−1143.

(24) Dahan, N.; Gorodetski, Y.; Frischwasser, K.; Kleiner, V.; Hasman, E. Geometric Doppler Effect: Spin-Split Dispersion of Thermal Radiation. *Phys. Rev. Lett.* **2010**, *105*, 136402.

(25) Lin, Y. H.; Chen, M. S.; Lin, W. C.; Tsou, Y. S. A polarization-independent liquid crystal phase modulation using polymer-network liquid crystals in a 90° twisted cell. *J. Appl. Phys.* **2012**, *112*, 024505.

DOI: 10.1021/acsphotonics.5b00536
ACS Photonics 2016, 3, 124−129